NASA/TM—2018–000000

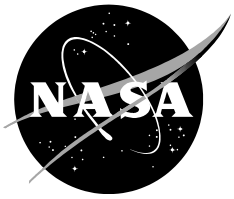

TESS Data Release Notes:
Sector 2, DR2

Michael M. Fausnaugh
Kavli Institute for Astrophysics and Space Science, Massachusetts Institute of Technology, Cambridge, Massachusetts

Douglas A. Caldwell
SETI Institute, Mountain View, California

Jon M. Jenkins
Ames Research Center, Moffett Field, California

Jeffrey C. Smith, Joseph D. Twicken
SETI Institute, Mountain View, California

Roland Vanderspek
Kavli Institute for Astrophysics and Space Science, Massachusetts Institute of Technology, Cambridge, Massachusetts

John P. Doty
Noqsi Aerospace Ltd, Billerica, Massachusetts

Jie Li
SETI Institute, Mountain View, California

Eric B. Ting
Ames Research Center, Moffett Field, California

Joel S. Villasenor
Kavli Institute for Astrophysics and Space Science, Massachusetts Institute of Technology, Cambridge, Massachusetts

---

December 5, 2018

Acknowledgements

These Data Release Notes provide information on the processing and export of data from the Transiting Exoplanet Survey Satellite (TESS). The data products included in this data release are target pixel files, light curve files, collateral pixel files, full frame images (FFIs), cotrending basis vectors (CBVs), and Data Validation (DV) reports, time series, and associated xml files.

These data products were generated by the TESS Science Processing Operations Center (SPOC, Jenkins et al., 2016) at NASA Ames Research Center from data collected by the TESS instrument, which is managed by the TESS Payload Operations Center (POC) at Massachusetts Institute of Technology (MIT). The format and content of these data products are documented in the Science Data Product Description Document (SDPDD)[1]. The SPOC science algorithms are based heavily on those of the Kepler Mission science pipeline, and are described in the Kepler Data Processing Handbook (Jenkins, 2017).[2] The Data Validation algorithms are documented in Twicken et al. (2018) and Li et al. (2018). The TESS Instrument Handbook (Vanderspek et al., 2016) contains more information about the TESS instrument design, detector layout, data properties, and mission operations.

The TESS Mission is funded by NASA's Science Mission Directorate.

This report is available in electronic form at
http://https://archive.stsci.edu/tess/

[1] https://archive.stsci.edu/missions/tess/doc/EXP-TESS-ARC-ICD-TM-0014.pdf
[2] https://archive.stsci.edu/kepler/manuals/KSCI-19081-002-KDPH.pdf

1 Observations

TESS Sector 2 observations include physical orbits 11 and 12 of the spacecraft around the Earth. Data were collected over a 27.4 day period, and paused for 1.44 days during perigee passage while downloading data.

Table 1: Sector 2 Observation times

	UTC	TJD[a]	Cadence #
Orbit 11 start	2018-08-23 14:24:19	1354.10102	91186
Orbit 11 end	2018-09-05 15:39:51	1367.15347	100583
Orbit 12 start	2018-09-07 02:14:18	1368.59406	101620
Orbit 12 end	2018-09-20 00:19:52	1381.51460	110922

[a] TJD = TESS JD = JD - 2,457,000.0

The spacecraft was pointing at RA (J2000): 16.551°; Dec (J2000): −54.0160°; Roll: −139.5665°. Two-minute cadence data were collected for 16,000 targets, and full-frame images were collected every 30 minutes. See the TESS project Sector 2 observation page[3] for the coordinates of the spacecraft pointing and center field-of-view of each camera, as well as the detailed target list. Fields-of-view for each camera with all two-minute targets can be found at the TESS Guest Investigator Office observations status page[4].

1.1 Notes on Individual Targets

Four very bright stars (Tmag $\lesssim$ 2) with large pixel stamps were not processed in the photometric pipeline. Target pixel files with raw data are provided, but no light curves were produced. The affected TIC IDs are 80256524, 47552789, 238196512, and 38877693.

Two targets were erroneously placed on the wrong CCD in Camera 4. A target pixel file for each target is provided, although the raw pixel data does not contain the target designated in the file names. No optimal apertures or light curves were produced. The affected TIC IDs are 374942153 and 350433330.

Two targets (214664575 and 300015238) have very bright stars nearby (214664574 and 300015239, respectively). The contaminating flux for these objects is very large and the pipeline assigns them disjoint photometric apertures, which likely causes uncorrected systematic errors in the light curves. Two other targets, 231005052 and 231005905, suffer from a similar problem except they are nearly the same brightness (Tmag ∼5.1).

One target (230981971) had a small aperture selected (25x25 pixels) that did not fully capture the bleed trails.

1.2 Spacecraft Pointing and Momentum dumps

As in Sector 1, the reaction wheel speeds were reset to low values with momentum dumps every 2.5 days. Cadences during momentum dumps have bit 6 set (Reaction Wheel desatu-

[3] https://tess.mit.edu/observations/sector-2

[4] https://heasarc.gsfc.nasa.gov/docs/tess/status.html

ration Event) and bit 8 set (Manual Exclude). These intervals include a 20 minute buffer for Fine Pointing mode to resume.

Figure 1 summarizes the pointing performance over the course of the sector based on Fine Pointing telemetry. The sudden decreases in dispersion every 2.5 days mark the momentum dumps.

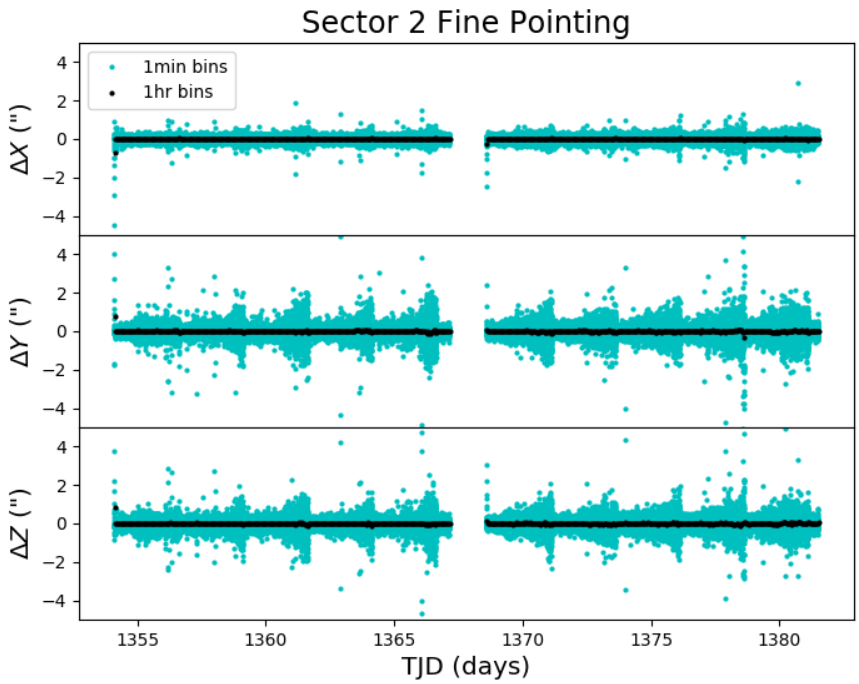

Figure 1: Guiding corrections based on spacecraft fine pointing telemetry. The delta-quaternions from each camera have been converted to spacecraft frame, binned to 1 minute and 1 hour, and averaged across cameras. Long-term trends (such as those caused by differential velocity aberration) have also been removed. The ΔX/ΔY directions represent offsets along the the detectors' rows/columns, while the ΔZ direction represents spacecraft roll. The sudden decrease in the dispersion every 2.5 days marks the momentum dumps.

1.3 Scattered Light

Figure 2 shows the median value of the background estimate for all targets on a given CCD as a function of time. Figure 3 shows the angle between each camera's boresight and the Earth or Moon—this figure can be used to identify periods affected by scattered light and the relative contributions of the Earth and Moon to the image backgrounds. In Sector 2, the main stray light features to be aware of are:

1. The upturns at the end of each orbit are caused by the Earth rising above the sunshade, which reaches a minimum of ∼50 degrees from the center of Camera 1. The Earth's daily rotation is evident in the background level.

2. The lower level rise in the first orbit of Camera 1 (days 4–9) is caused by the Moon moving within 30 degrees of the camera boresight.

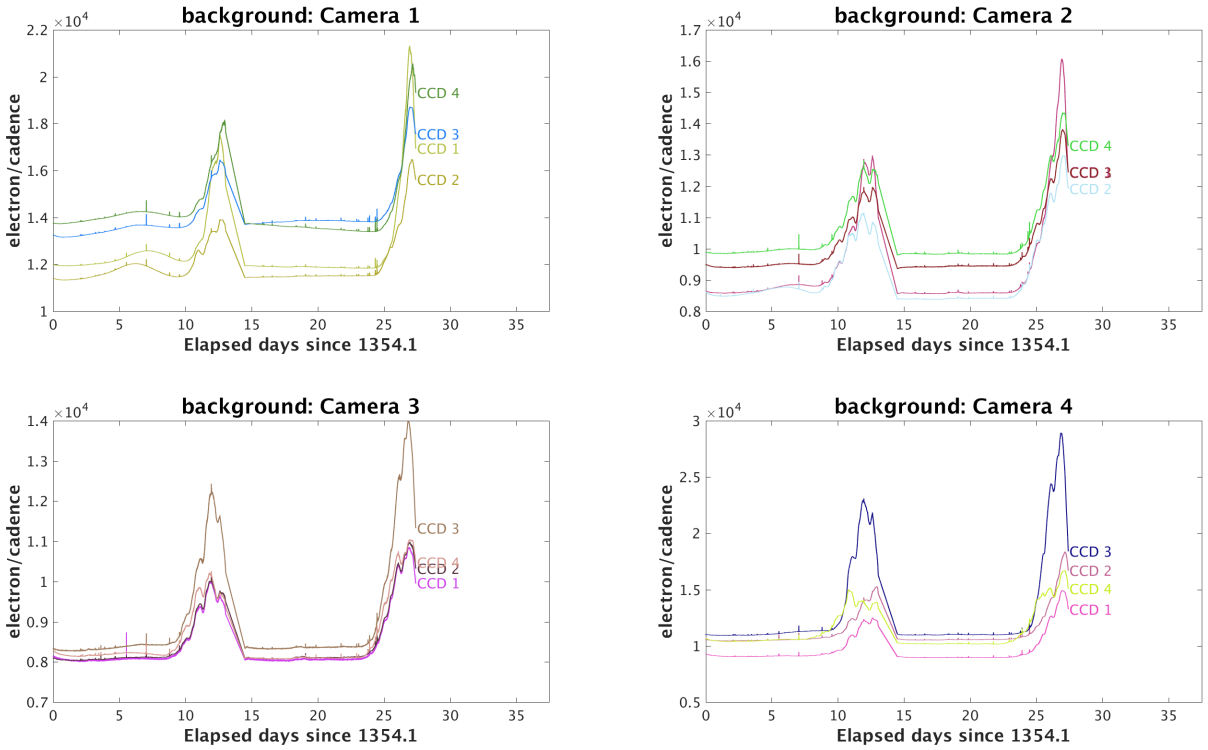

Figure 2: Median background flux across all targets on a given CCD in each camera. The changes are caused by variations in the orientation and distance of the Earth and Moon. The upturn at the end of each orbit is caused by the Earth rising above the sunshade.

2 Data Anomaly Flags

See the SDPDD (§9) for a list of data quality flags and the associated binary values used for TESS data, and the instrument handbook for a more detailed description of each flag.

The following flags were not used in Sector 2: bits 1, 2, 7, 9, 11, and 12 (Attitude Tweak, Safe Mode, Cosmic Ray in Aperture, Discontinuity, Cosmic Ray in Collateral Pixel, and Straylight).

Cadences marked with bits 3, 4, and 6 (Coarse Point, Earth Point, and Reaction Wheel Desaturation Event) were marked based on spacecraft telemetry.

Cadences marked with bit 5 and 10 (Argabrightening Events and Impulsive Outlier) were identified by SPOC pipeline results. Bit 5 marks a sudden change in the background measurements. In practice, all bit 5 flags are caused by the unstable pointing at times near momentum dumps. Bit 10 marks an outlier identified by PDC and omitted from the cotrending procedure.

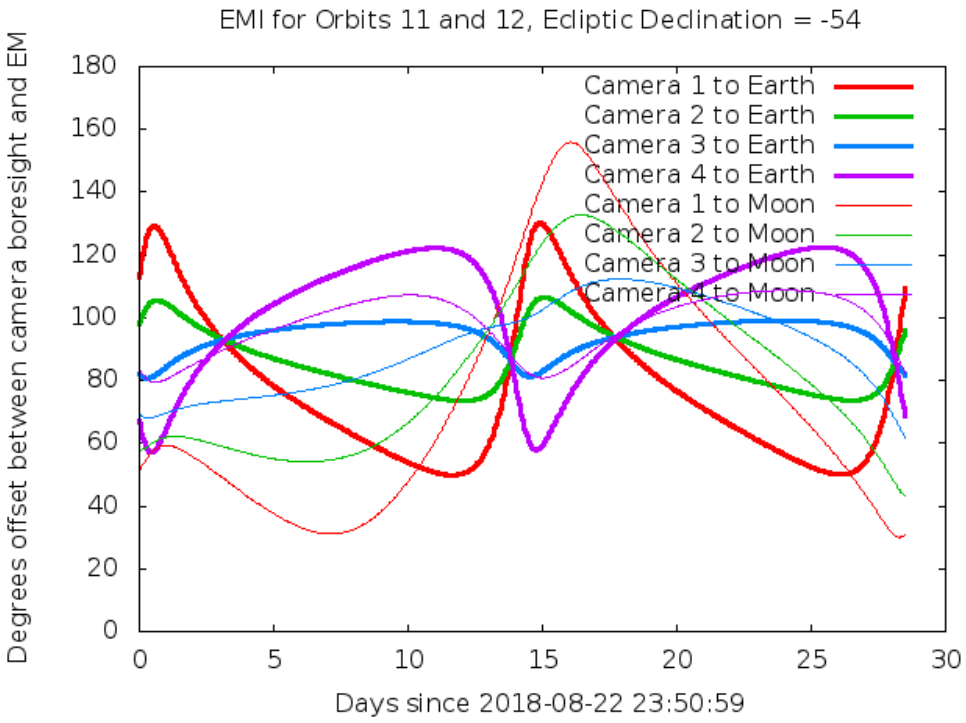

Figure 3: Angle between the four camera boresights and the Earth/Moon as a function of time. When the Earth/Moon moves within 37° of a camera's boresight, scattered light patterns and complicated features such as glints may appear. At larger angles, low level patchy features may appear. This figure can be used to identify periods affected by scattered light and the relative contributions of the Earth and Moon to the background. However, the background intensity and locations of scattered light features depend on additional factors, such as the Earth/Moon azimuth and distance from the spacecraft.

Cadences marked with bit 8 (Manual Exclude) are ignored by PDC, TPS, and DV for cotrending and transit searches. In Sector 2, these cadences were identified using spacecraft telemetry from the fine pointing system. All cadences with pointing excursions >21 arcseconds (∼1 pixel) were flagged for manual exclude. This procedure predominantly flags cadences just before and during each momentum dump, and results in nearly the same selection as would have been identified by the procedure described in the Sector 1 data release notes. See Figure 4 for an assessment of the performance of the detrending based on the final set of manual excludes.

FFIs were only marked with bit 6 (Reaction Wheel Desaturation Events). Only one or two FFIs are affected by each momentum dump.

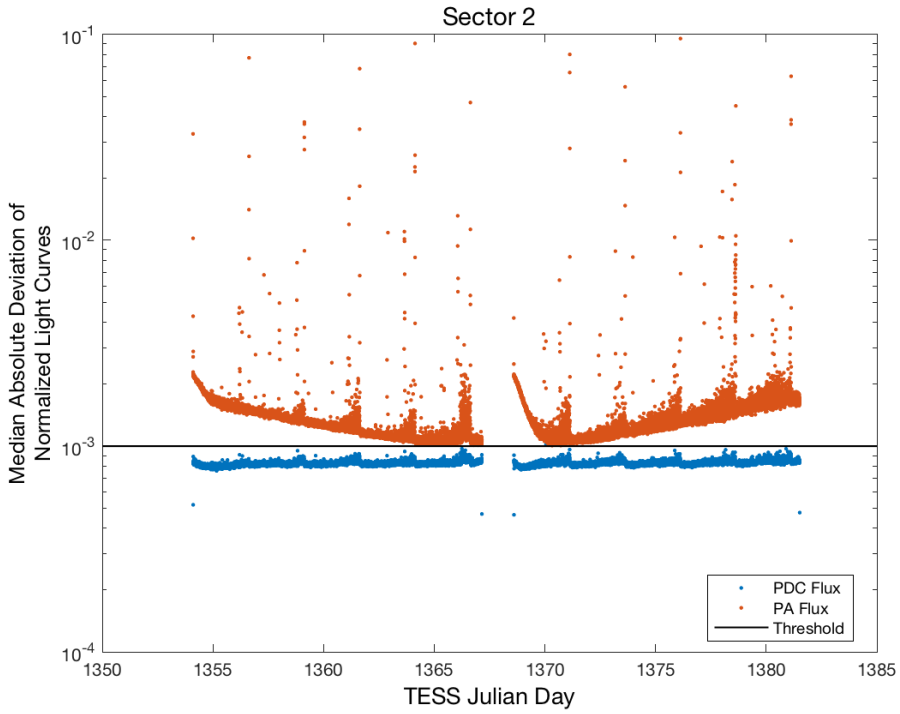

Figure 4: Median absolute deviation (MAD) for the 2-minute cadence data from Sector 2, showing the performance of the cotrending after identifying Manual Exclude data quality flags. The MAD is calculated in each cadence across stars with flux variations less than 1% for both the PA (red) and PDC (blue) light curves, where each light curve is normalized by its median flux value. The scatter in the PA light curves is much higher than that for the PDC light curves, and the outliers in the PA light curves are largely absent from the PDC light curves due to the use of the anomaly flags. Note that the MAD for some of the cadences in the PDC light cuves have values slightly above 1×10^{-3} threshold after reprocessing. Note also that the first and last cadences in each orbit are treated as gaps by PDC.

3 Anomalous Effects

3.1 Smear Correction Issues

1. Camera 2, CCD 2, Column 1930: There is a bright star in the bottom buffer rows (barely visible in the science imaging region) bleeding into the frame store and affecting the smear correction.

2. Camera 4, CCD4, Column 584: A bright star is located in the upper buffer rows, which bleeds into the upper serial register. The associated undershoot affects the smear correction of adjacent columns.

3. Camera 1, CCD4, Column 812 and Camera 2, CCD 3, Column 778: The virtual rows are consistent with saturated stars in the lower buffer rows slightly bleeding into the frame store.

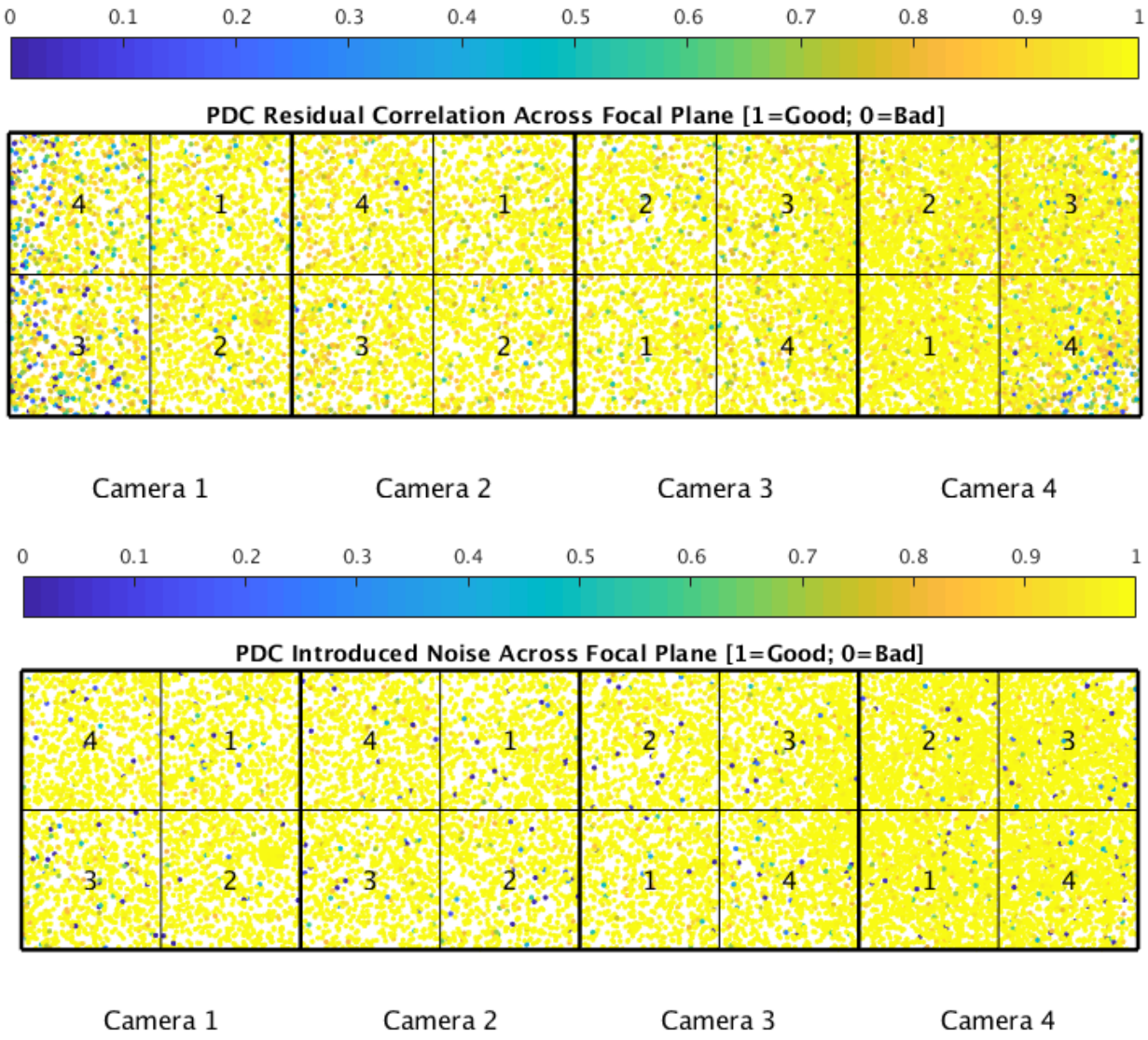

Figure 5: PDC residual correlation goodness metric (top panel) and PDC introduced noise goodness metric (bottom panel). The metric values are shown on a focal plane map indicating the camera and CCD location of each target. The correlation goodness metric is calibrated such that a value of 0.8 means there is less than 10% mean absolute correlation between the target under study and all other targets on the CCD. The introduced noise metric is calibrated such that a value of 0.8 means the power in broad-band introduced noise is only slightly above the level of uncertainties in the flux values.

3.2 Black Flutter

Flutter in the mean black level was observed in Camera 1, CCD 2, cadences 92650 to 93300 and cadences 109600 to 110922. The same effect was seen in Camera 4, CCD 2, cadences 103070 to 105750. See the instrument handbook for more details about overclock flutter.

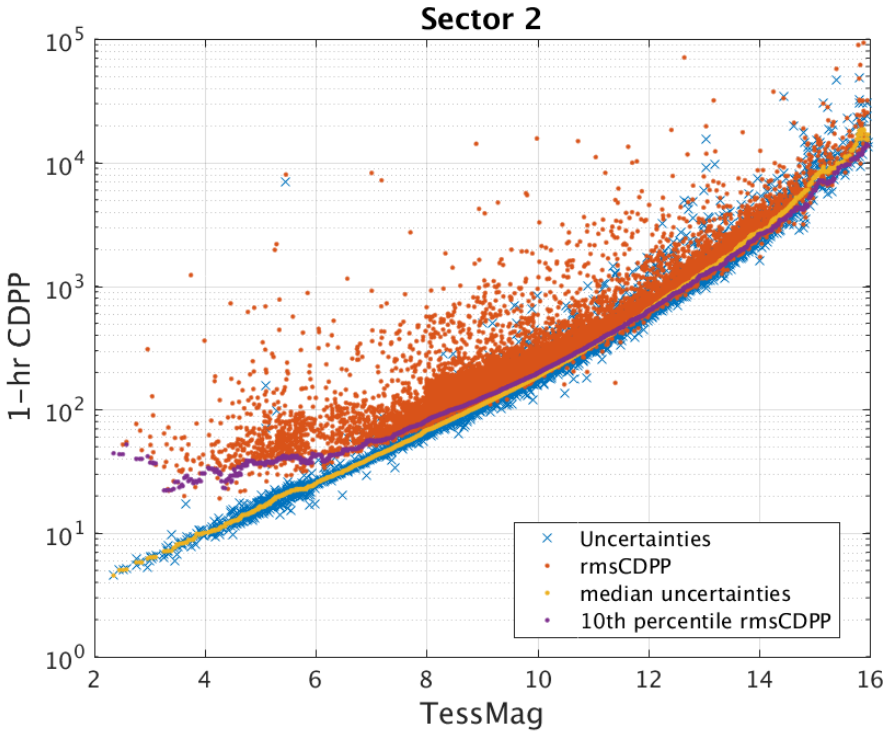

Figure 6: 1-hour CDPP. The red points are the RMS CDPP measurements for the 15,994 light curves from Sector 2 plotted as a function of TESS magnitude. The blue x's are the uncertainties, scaled to 1-hour timescale. The purple curve is a moving 10th percentile of the RMS CDPP measurements, and the gold curve is a moving median of the 1-hr uncertainties.

3.3 Fireflies and Fireworks

Table 2 lists all firefly and fireworks events for Sector 2. These phenomena are small, spatially extended, comet-like features in the images that may appear one or two at a time (fireflies) or in large groups (fireworks). See the instrument handbook for a complete description.

Table 2: Sector Fireflies and Fireworks

FFI Start	FFI End	Cameras	Description
2018236165941	2018236172941	2	single firefly
2018239045941	2018239052941	3	single firefly
2018241025941	2018241035941	1, 2, 3, 4	fireworks

4 Pipeline Performance and Results

4.1 Light Curves and Photometric Precision

Figure 5 gives the PDC goodness metrics for residual correlation and introduced noise on a scale between 0 (bad) and 1 (good). The performance of PDC is very good and generally uniform over most of the field of view. As in data release 1, the goodness metrics reported in the light curve files are uncalibrated and should not be considered reliable–the calibrated goodness metrics are shown in Figure 5 and available in a supplemental file with these release notes.

Figure 6 shows the achieved Combined Differential Photometric Precision (CDPP) at 1-hour timescales for all targets. As in Sector 1, the dominant systematic uncertainty is pointing jitter.

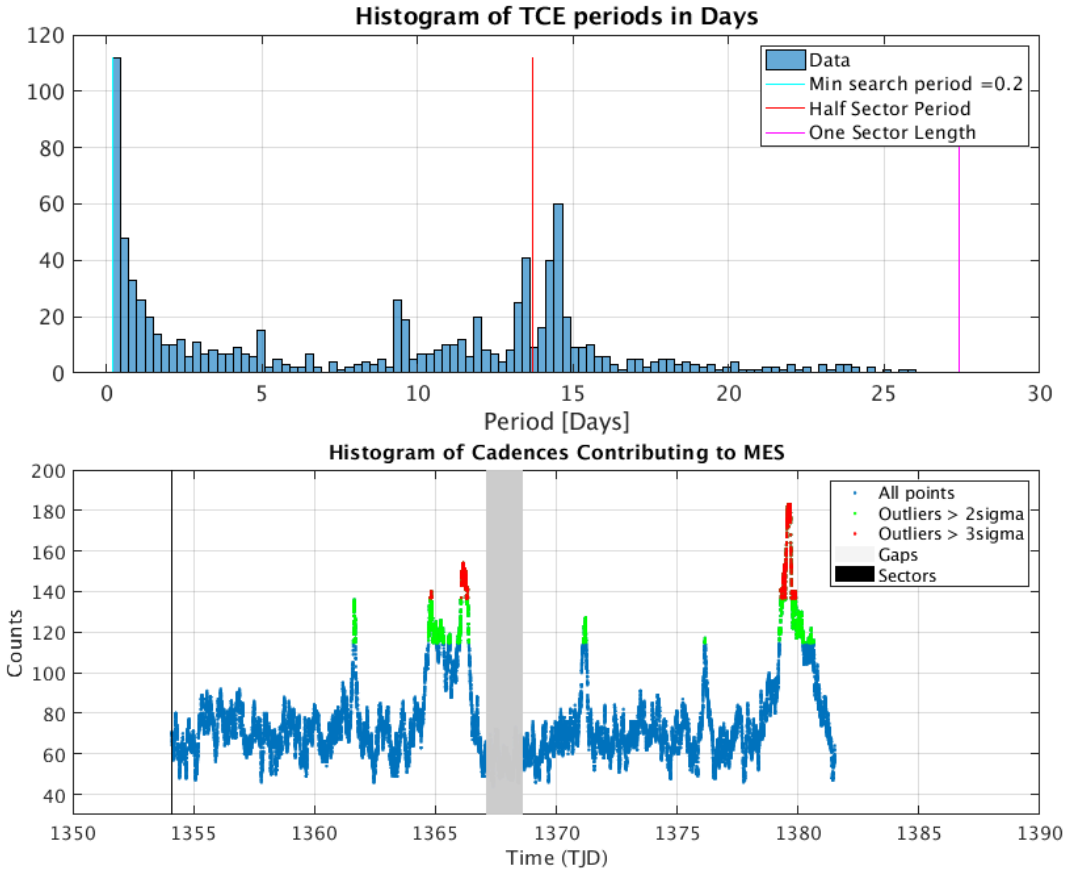

Figure 7: Top Panel: Histogram of orbital periods for 1348 TCEs identified in TPS in Sector 2. Bottom Panel: Number of TCEs at a given cadence exhibiting a transit signal. Isolated peaks are caused by a single event and result in spurious TCEs. Here, the peaks align with momentum dumps that are spaced at integer multiples of 2.5 days. This accounts for the narrow spikes in the histogram at 5, 10, 12.5, and 15 days. The larger spikes at TJD ∼1366 and ∼1379 days are caused by scattered light features (see §1.3) and account for the peak in the histogram between 13 and 14 days.

4.2 Transit Search and Data Validation

In Sector 2, the light curves of 15,994 targets were subjected to the transit search in TPS. Of these, Threshold Crossing Events (TCEs) at the 7.1σ level were generated for 906 targets.

The top panel of Figure 7 shows the distribution of orbital periods for the TPS TCEs found in Sector 2. Narrow peaks in the histogram occur at approximately 5, 10, 12.5, and 15 days. These periods are integer multiples of the 2.5 day period between momentum dumps, and are mainly caused by pointing excursions and gaps in the light curves that appear with approximately the same frequency. This is confirmed by the bottom panel of Figure 7, which shows the number of TCEs at a given cadence that exhibit a transit signal—the isolated peaks are close to the times of momentum dumps.

There is also an excess of TCEs between approximately 13 and 14 days, around the orbital period of TESS. These TCEs are generally caused by scattered light effects after the Earth rises above the sunshade (see §1.3), and can be identified with the large ($>3\sigma$) peaks in the bottom panel of Figure 7. In these cases, there are usually gradients across the target pixels or a sudden sharp feature that moves through the field of view. Note that these TCEs can appear as very credible shallow transits—inspection of the images (e.g., the in-/out-of-transit difference images in the full DV reports) is required to show that these TCEs are actually false positives.

A search for additional TCEs in potential multiple planet systems was conducted in DV through calls to TPS. A total of 1348 TCEs were ultimately identified in the SPOC pipeline on 906 unique target stars. Table 3 provides a breakdown of the number of TCEs by target. Note that targets with large numbers of TCEs are likely to include false positives.

Table 3: Sector 2 TCE Numbers

Number of TCEs	Number of Targets	Total TCEs
1	590	590
2	224	448
3	70	210
4	14	56
5	4	20
6	4	24
–	906	1348

Figure 8 shows the distribution of transit depths derived from limb-darkened transiting planet model fits for TCEs with SNR $> 7.1\,\sigma$. The model transit depths range down to the order of 100 ppm, but the bulk of the transit depths are considerably larger.

References

Jenkins, J. M. 2017, Kepler Data Processing Handbook: Overview of the Science Operations Center, Tech. rep., NASA Ames Research Center

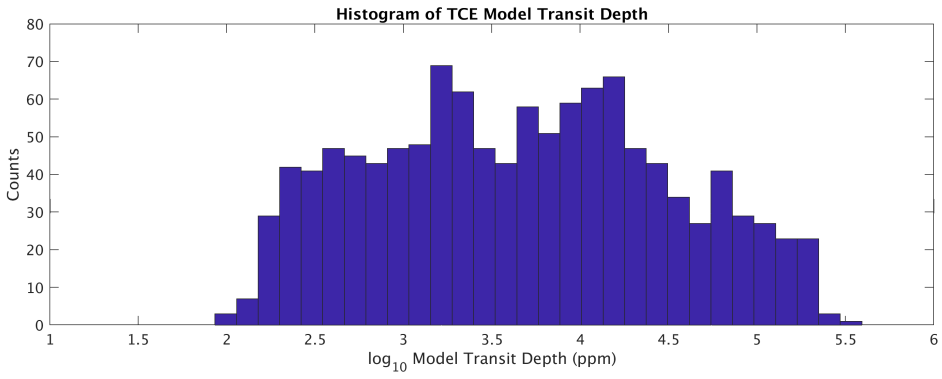

Figure 8: Histogram of limb-darkened transiting planet model transit depth for 1348 TCEs with SNR $> 7.1\,\sigma$. Transit depth is displayed on a logarithmic scale in units of ppm.

Jenkins, J. M., Twicken, J. D., McCauliff, S., et al. 2016, in Proc. SPIE, Vol. 9913, Software and Cyberinfrastructure for Astronomy IV, 99133E

Li, J., Tenenbaum, P., Twicken, J. D., et al. 2018, ArXiv e-prints, arXiv:1812.00103

Twicken, J. D., Catanzarite, J. H., Clarke, B. D., et al. 2018, *PASP*, 130, 064502

Vanderspek, R., Doty, J., Fausnaugh, M., & Villaseñor, J. 2016, TESS Instrument Handbook, Tech. rep., Kavli Institute for Astrophysics and Space Science, Massachusetts Institute of Technology